X-Spec, A Multi-Object, Trans-Millimeter-Wave Spectrometer for CCAT

C.M. Bradford[a], S. Hailey-Dunsheath[b], E. Shirokoff[b,c], M. Hollister[b], C.M. McKenney[b], H.G. LeDuc[a], T. Reck[a], S.C. Chapman[d], A. Tikomirov[d], T. Nikola[e], J. Zmuidzinas[b]

[a]Jet Propulsion Laboratory, Pasadena, CA, USA
[b]California Institute of Technology, Pasadena, CA, USA
[c]University of Chicago, Kavli Institute for Cosmological Physics, Chicago IL, USA
[d]Dalhousie University, Halifax, Nova Scotia, CANADA
[e]Cornell University, Ithaca, NY, USA

ABSTRACT

We present the result of a design study for X-Spec, a multi-beam, R=400–700 survey spectrometer covering 190–520 GHz under development for CCAT. It is designed to measure the bright atomic fine-structure and molecular rotational transitions that cool galaxies' interstellar gas, in particular, the 158 μm rest-frame [CII] transition, in thousands to tens of thousands of galaxies ranging from z=9 to z=3.5. With the wide bandwidth and multi-object capability, X-Spec / CCAT will be more powerful than ALMA for redshift-blind galaxy surveys and tomographic intensity mapping. X-Spec uses SuperSpec filterbank spectrometer technology with TiN KIDs described by Hailey-Dunsheath et al. in this conference. Because the density of sources is small, galaxy follow-up will be most efficient with a front-end steering unit which we have prototyped, also described in a separate paper (Chapman et al. in this conference). Our baseline instrument concept has 84 steered beams arrayed over the 1 degree CCAT field, each beam couples to 4 chips (2 bands x 2 polarizations) each chip with approximately 500 detectors, making a total of ∼170,000 KIDs in the full instrument. A direct imaging spectrometer (integral-field spectrometer) with a comparably-sized backend is also considered.

Keywords: CCAT, Submillimeter Spectroscopy, Multi-Object Spectroscopy, [CII] Tomography, Filterbank, Kinetic Inductance Detector

1. INTRODUCTION – SCIENTIFIC LANDSCAPE

1.1 Cosmic star-formation history, role of dust-obscured sources

The epoch of reionization, and the birth and subsequent growth of galaxies and clusters in the first half of the Universe's history are key topics in modern astrophysics. Unfortunately, the bulk of our information about this important epoch comes from studies in the rest-frame ultraviolet (UV) and optical (e.g. Bouwens et al.[2]). Yet measurement of the cosmic far-IR background[3] indicates that in aggregate, most of the energy released by stars and accreting black holes through the Universe's history has been absorbed and reradiated by dust (Figure 1). Space-borne submillimeter (submm) and ground-based millimeter (mm) surveys have found the brightest of these dusty galaxies, they are similar to our local-universe luminous and ultra luminous infrared galaxies (LIRGs, ULIRGs) but extend back to z>6. As with the LIRGs and ULIRGs, in these dusty galaxies the ultraviolet is a tiny fraction of the total luminosity (0.2–17%), and even when corrections are applied based on UV spectral slopes, the total luminosities are underestimated by typical factors of 3–100, see for example the right panel of Figure 1.

A complete measure of the history of galaxies requires probes of both bolometric luminosity and physical conditions which are unbiased by dust obscuration. Continuum imaging in the far-IR and submillimeter is well underway, and will be brought to a high level of maturity with the speed and angular resolution of the CCAT and other facilities. However, continuum imaging alone is deficient in two critical aspects: it does not provide redshifts, and it offers only small insight into the conditions where energy is released at the heart of the dust-obscured sources.

Send correspondence to C.M.B.: E-mail: bradford@caltech.edu, Telephone: 1 818 726 8622

Millimeter, Submillimeter, and Far-Infrared Detectors and Instrumentation for Astronomy VII, edited by Wayne S. Holland, Jonas Zmuidzinas, Proc. of SPIE Vol. 9153, 91531Y · © 2014 SPIE · CCC code: 0277-786X/14/$18 · doi: 10.1117/12.2056750

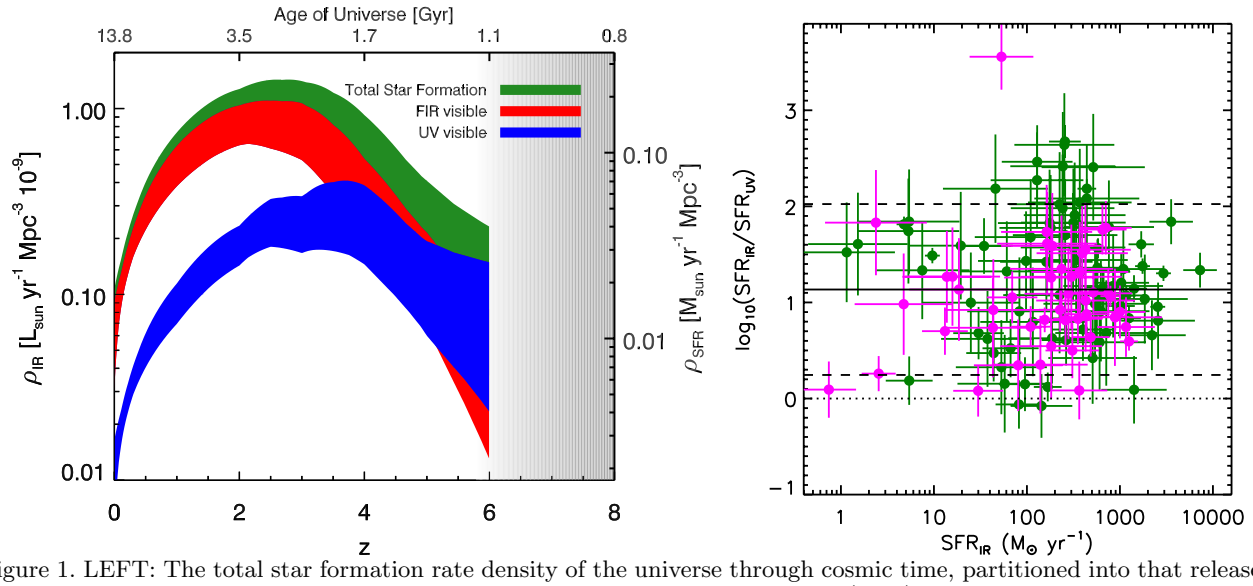

Figure 1. LEFT: The total star formation rate density of the universe through cosmic time, partitioned into that released in the UV and that released in the far-IR. Data are based on Bouwens et al. (2009) and updated based on Casey et al. (2013) and Plank data. The bulk of the stellar populations were built up near the peak, where star formation was dominated by dust-obscured systems. Note that the far-infrared probes the vast majority of the star formation at z<6, and that there is a clear transition in the role of dust obscured star formation at 4<z<6, a region which CCAT will uniquely probe. RIGHT: Factor by which the UV-based estimate of the star formation rate falls short of that measured with the submillimeter photometry in SCUBA-2 galaxies (from Casey et al., 2013[1]). Green points are sources detected at 450 μm while magenta points are sources detected at 850 μm but not 450 μm. On average, the star formation rates calculated from templates in the UV/optical/near-infrared underestimate the star formation rate of these SMGs by factors of ∼13, but the underestimates range up to factors of >100. Note that the UV/optical/near-infrared estimates are already corrected for dust extinction.

1.2 Redshift Surveys with X-Spec

With its broad 190–520 GHz spectral coverage, X-Spec is able to measure redshifts throughout the history of galaxies. The band accesses the CO rotational ladder at low to intermediate redshifts, as was used with Z-Spec,[4] then shifts to the powerful [CII] fine-structure transition at z>3.5. The fact that [CII] is such a powerful line means that the X-Spec redshift sensitivity is uniquely capable at the early times. Figures 2 shows example galaxy spectra with X-Spec sensitivities, and illustrates the X-Spec redshift capability.

We outline an example program targeting the optically inaccessible sources in which ∼100 spectroscopic redshifts are obtained in each of 5 redshift × 5 luminosity bins, extending down to L∼ 3×10^{11} $L_\odot$. The 100 samples per bin ensures that the uncertainty in physical parameters in each bin is <0.05 dex. Adopting the mean sensitivity when weighted by log(1 + z) over the range from z=1 to z=9 (corresponding to SNR of 20 for the source and integration time plotted in the lower panel of Figure 2), the L∼ 3×10^{11} $L_\odot$ source is detectable (4σ) in ∼48 hours if simply scaled with luminosity. Budgeting this depth for all 2500 galaxies (a conservative assumption) thus requires 7000 beam-nights on CCAT, or ∼ 80 nights with the 84-spectrometer first light system at goal sensitivity. Table 1 summarizes this and the other observational goals.

1.3 Probing Interstellar Conditions

A second, crucial, limitation of the continuum datasets is that with the exception of very warm dust (>100 K) signaling accretion power, the dust continuum carries very little information regarding the underlying energy sources. The dust is, after all, only ∼1% of the interstellar medium (ISM) fueling new stars and accreting black holes. The gas phase can in principle be probed with UV/optical/near-IR spectroscopy, but for sources with substantial dust content, this only probes a thin skin, missing the bulk of the activity in an obscured galaxy. The suite of far-IR lines probe all phases of the interstellar medium, and the negligible optical depth of galaxies at far-IR wavelengths ensures that even the most heavily embedded regions where stars form and black holes grow are revealed. For the atomic and ionized medium, the key far-infrared emission lines are those of C, N,

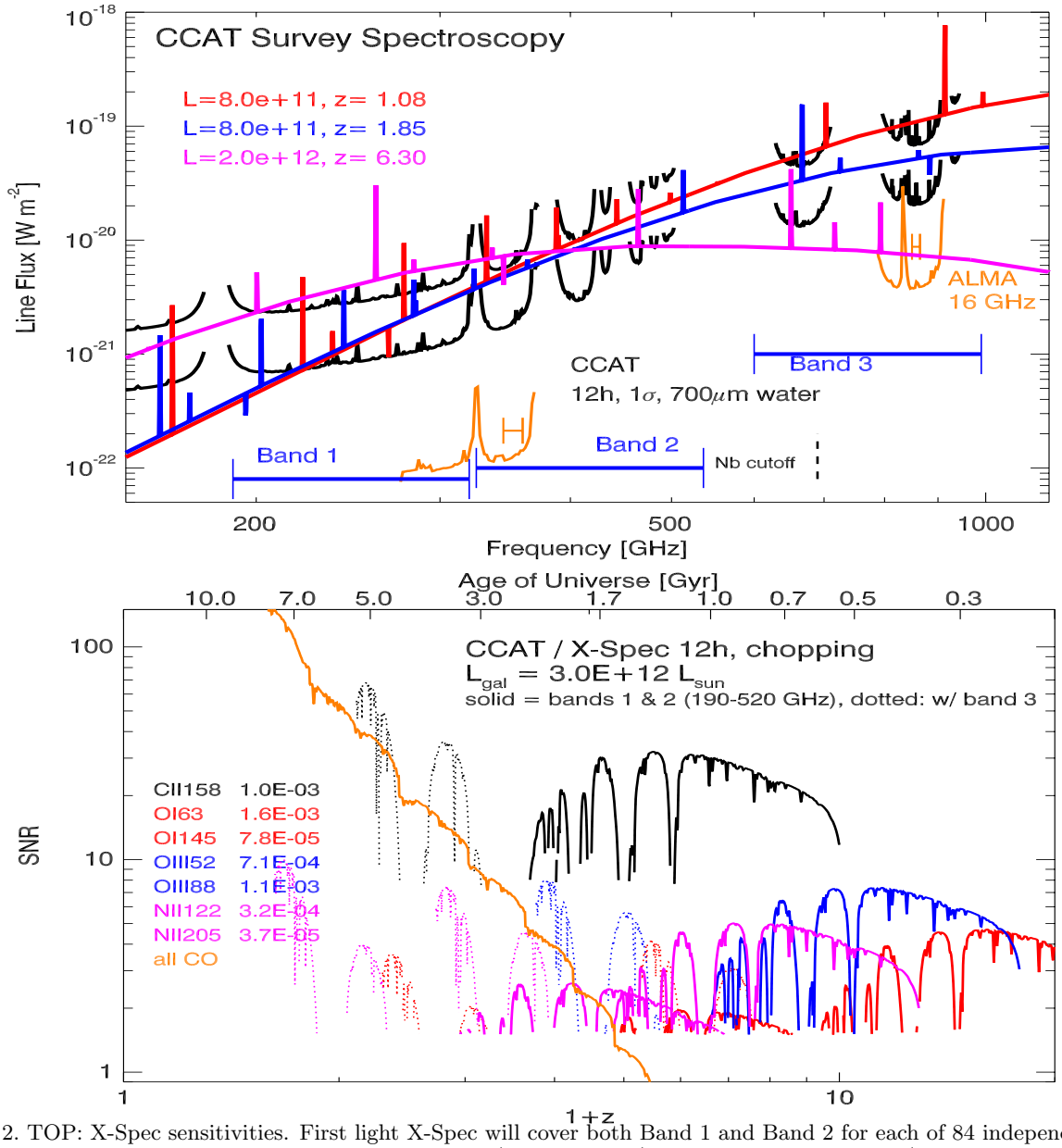

Figure 2. TOP: X-Spec sensitivities. First light X-Spec will cover both Band 1 and Band 2 for each of 84 independently-steered feeds. The upper curve shows an upper limit to (worst case for) the first-light sensitivity (single pol, 2× photon noise limited, line extracted from a total effective bandwidth of R=250), while the lower curve is the goal (dual pol, $\sqrt{2}\times$ photon noise, effective noise bandwidth of R=700). For both cases, we assume an end-to-end instrument efficiency of 25%, a 92% forward efficiency (a conservative 8% warm loading), an 85% taper efficiency (total maximum aperture efficiency of 78%), and the Ruze efficiency factor for a surface RMS of 10 microns. The sky is assumed to have 400 μm of precipitable water vapor and be viewed at a 40° zenith angle. For comparison, Z-Spec on the CSO obtained 1 σ sensitivities in fitted line fluxes of $\sim 6 \times 10^{-21}$ W m^{-2}, when scaled to the 12 hours and 25-meter telescope. BOTTOM: Signal-to-noise ratio (SNR) of a galaxy through cosmic time obtained with CCAT / X-Spec observing the CO and fine-structure transitions. Fine-structure line fractional luminosities are taken from Spinoglio et al. (2012);[5] they are based on local-universe galaxies and carry scaling with galaxy luminosity. The CO fractional luminosities are from Visbal and Loeb (2011)[6] and are fixed with luminosity. The heavy black curve shows the sensitivity to [CII] from from z=9 to 3.

& O: (e.g., [OI] 63 μm, 146 μm, [CII] 158 μm, and [OIII] 52 μm, 88 μm, [NIII] 57 μm, and [NII] 122 μm, 205 μm). The emitting species cover more than an order of magnitude in ionization potential and they strongly constrain the density and temperature of the ionized and neutral gas, and the strength and hardness of the interstellar

Table 1. CCAT X-Spec Example Surveys

Goal	Depth [$L_\odot$]	f_{line} / $f_{[CII]}$	SNR	t_{int} [h]	N	mnts w/ 84
[CII] and CO z survey	3e11	1	4	48	2500	3.0
stacked ISM diagnostics	3e11	0.1	0.4	48	2500	done
Deep [CII] / CO stack w/ OIR redshifts	5e10	1	0.4	17	10,000	4.3
20-sq degree clustering survey	5e11	1	3	10	12,000	2.9
[CII] tomography first light, linear strips, 4 redshift bins, 600 hours						1.3
[CII] tomography full field, cross correlate with with LOFAR [HI], 4000 hours						8.3

Notes: t_{int} is the integration time per object. f_{line} / $f_{[CII]}$ is the line fractional luminosity relative to [CII] at high redshifts, or mid-J CO at low redshifts. mnts w/ 84 is the number of months required on CCAT with the proposed 84-steered-beam X-Spec.

radiation field. These physical parameters then reveal the relative importance of the black hole vs. the hot young stars to the overall energy budget, and measure the top of the stellar mass function.

In particular, the [CII] 158 μm transition is often the brightest single line in the spectrum of a star-forming galaxy, emitting as much as 0.5–1% of the total FIR luminosity.For the highest redshift systems where [CII] line emission is detected, the ratio of its luminosity to the total bolometric luminosity (provided automatically with the continuum surveys) can be used as a diagnostic tool that provides: (1) a measure of the star-formation activity, (2) a measure of the spatial extent (or 'mode) of star formation, and (3) an AGN/starburst discriminant.[7–10]

Spectral Stacking / Cross Correlation Analyses. X-Spec surveys will also access the other fine-structure transitions. The fainter lines will be individually detected in luminous systems, but the real power will likely come through stacking analyses. As an example, consider the 2500-object redshift survey described above. Each of the 100-galaxy bins, when spectrally stacked using a priori redshifts, would provide an effective factor of 10 increase in sensitivity, thereby detecting the [NII] 205 μm line and perhaps high-J CO for the intermediate redshifts (z$\sim$2.5–4), and the [OIII] 88, [NII] 122 μm and possibly [OI] 145 μm for the higher redshifts (see Table 1, line 2). These stacked datasets are more powerful than a handful of very deep integrations to provide individual detections, as they provide aggregate measures of the conditions in each luminosity class and redshift interval. The complete survey will therefore chart the cosmic history of UV field hardness and ISM density. A priori redshifts can come from X-Spec via [CII] or CO, but the potential sample for this kind of analysis is much broader. Optical/near-IR redshift surveys (e.g. Subaru Prime-Focus- Spectrograph, BigBOSS, and Euclid), for example, will produce millions of sources at intermediate redshifts ($0.5 < z < 3$), for which X-Spec stacked spectra will provide the definitive molecular gas census with the CO rotational ladder (Table 1, line 3).

1.4 Tomographic intensity mapping: reionization and large-scale structure

The epoch of reionization (EoR) represents a major transition in the history of the cosmos; it is the first chapter in the history of galaxies and heavy elements marked by the onset of the first generation of stars. Detecting the individual primordial galaxies responsible for reionization is difficult as they are believed to be intrinsically low-mass, low-bolometric-luminosity objects. Extremely deep imaging with the Hubble Space Telescope (HST) has begun to probe the very bright end of the UV luminosity functions at $z > 6$,[11] with improvements anticipated with the James Webb Space Telescope (JWST). However, neither of these space-borne facilities nor CCAT nor ALMA is expected to resolve the majority of sources responsible for reionization at $z > 8$.[12]

Rather than target individual galaxies, another approach is to survey a piece of sky with a spectrometer, creating a 3-D data volume in which the line-of-sight dimension is mapped to frequency for a narrow spectral feature. The fluctuations in this volume are due primarily to undetected line emission in galaxies, and the fluctuation power as a function of spatial frequency carries information about the galaxies' properties, even though they are not individually detected. The tomographic or (3-D) intensity mapping technique has been studied theoretically.[13–18] The 200–400 GHz band conveniently corresponds to z=4–9 for [CII], making the millimeter band a natural probe of reionization. In the long term, later-generation version of X-Spec with a field-filling IFU will fully sample a few-square-degree piece of sky as described in Gong et al. 2012,[19] and this will be a powerful complement to the HI 21-cm line intensity mapping[20–22] that trace the neutral medium at $z > 6$ (e.g., PAPER, MWA, LOFAR). The [CII] data cubes can be cross-correlated with HI 21-cm datasets data to trace the bubble size and ionization history of the intergalactic medium.

In the near term, we are studying more modest [CII] tomography experiments, including the TIME-Pilot experiment described in these proceedings by A. Crites et al. The X-Spec instrument described in this paper,

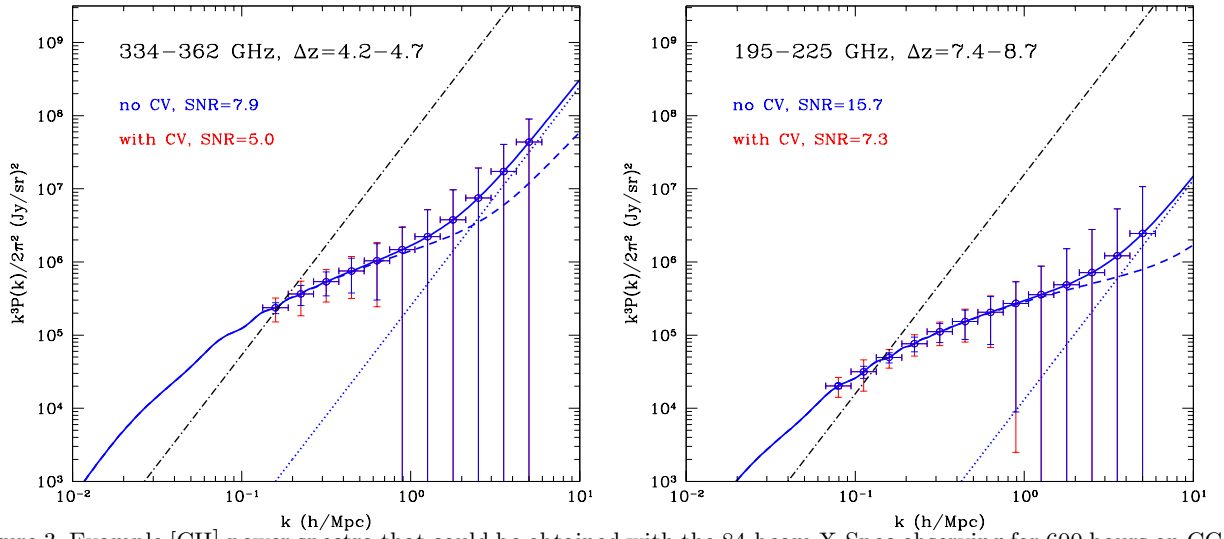

Figure 3. Example [CII] power spectra that could be obtained with the 84-beam X-Spec observing for 600 hours on CCAT. The experiment is carried out by aligning the spectrometer beams into 7 lines on the sky, then scanning the telescope back and forth with an 0.8-degree slew. Each power spectrum has two basic components. At high k the spectrum shows shot or Poisson noise due to the discrete nature of individual galaxies, this creates a k^3 dependence in these units. At low k, the spectrum shows galaxy clustering, or large-scale structure which offers a probe of the total [CII] emission in the Universe. Calculations by Y. Gong.

deployed on a telescope like CCAT would offer a powerful advance following TIME-Pilot; Figure 3 shows example 3-D [CII] power spectra that could be obtained in a straw man 600-hour survey. Here we assume that the steering units can be used to orient the spectrometers into lines on the sky, then slewing the telescope back and forth along the direction of these lines. This concentrates the sensitivity into strips one beam wide by ∼1 degree in length. As for TIME-Pilot, the long line provides sensitivity to the low-k modes, and the sensitivity concentration provided by the line scan offers improves the SNR.

As Crites et al. note, CO emission from lower-redshift galaxies will likely dominate the fluctuations, so these galaxies will need to be masked from the survey volume using prior information (e.g. from near-IR photometric or spectroscopic redshifts) to recover the [CII] spectrum. Since the number of 3-D pixels ('voxels') in the survey volume scales inversely with the beam size and spectral bin width, a larger telescope and higher-resolution spectrometer (X-Spec / CCAT) will offer greater flexibility in masking the intermediate-z CO emitters.

1.5 Comparison with ALMA

The galaxy-by-galaxy surveys described in Section 1.3 require spectra of thousands to tens of thousands of galaxies. While ALMA will be powerful for studying hundreds of objects in great kinematic and morphological detail, it is not optimized for surveying. The bright transitions are approximately uniformly distributed in $\log \nu$, so ALMA measures only one bright transition at a time, and thus requires multiple tunings if redshifts are not known. Specifically, to completely cover the full X-Spec dual-band range (190–520 GHz) *requires 15 different ALMA tunings*. Without the bandwidth consideration, ALMA's sensitivity advantage 12–40× (less than the ratio in collecting area ratio because CCAT has higher atmospheric transmission and aperture efficiency, and the direct-detection spectrometers are slightly more sensitive than the ALMA receivers). If photometric redshifts are good enough such ALMA requires only 8 tunings for a redshift measurement (with ALMA 16 GHz, this requires δz=1.6, 2.4, 3.0 for z=4, 5, 6), then X-Spec at its goal sensitivity with 84 MOS units is 6 times faster than ALMA for galaxy surveys. Of course, if redshifts are known, the multiple ALMA tunings are not required, but then the secondary lines are not observed and are unavailable for inclusion in a stacking / cross-correlation measurement. Moreover, these estimates do not include the impact of the ALMA overhead for multiple pointings and tunings.

ALMA is even less well-suited to the tomography experiments. ALMA's only method of measuring clustering or total [CII] intensity is to identify and measure individual sources. Several dozen to a few hundred ALMA

detections in a 3-D volume can reveal the clustering length scales (the power spectrum shape). But absolute measurements, as required for extracting the total absolute [CII] intensity, require going deep enough to probe the bulk of the luminosity function, and doing so over a volume sufficient to overcome sample variance. Recovering the information contained in the X-Spec survey outlined in Figure 3, for example, requires ALMA to cover the same cosmological volume (a total of ∼0.02 square degrees, corresponding to ∼500 ALMA pointings × 150 GHz, corresponding to ∼10 ALMA tunings). The [CII] luminosity functions at this epoch of not well known, but if we adopt 10^8 $L_\odot$ for the minimum-[CII]-luminosity object that the survey will extract in order to probe the bulk of the luminosity function, and require a 3σ detection of this object at z=7, the integration time per beam per tuning is 1.1 hours with ALMA (again neglecting overheads). Thus the full ALMA survey requires on order 5000 hours, a factor of several longer than X-Spec. For more information, we refer the reader to Uzgil et al. 2014 (ApJ, in press), which includes a careful comparison between galaxy-by-galaxy surveys and tomography.

2. INSTRUMENT REQUIREMENTS AND APPROACH

Spectral Coverage. X-Spec will span the widest-possible bandwidth afforded by the atmospheric windows and the constraint of maintaining high efficiency. We identify 3 bands in Figure 2, each less than an octave so readily coupled to a single-mode feed. For first light we focus on Bands 1 and 2, spanning from 190–520 GHz. This combination provides good redshift sensitivity throughout cosmic time through the combination of CO and [CII], and is tractable with 2-layer anti-reflection coatings or structures.

Resolving Power. X-Spec is designed to detect and measure fluxes of weak gas-phase lines emanating from full galaxies, each of which lies within a CCAT beam. Spectral resolving power $\mathcal{R} = \nu/\delta\nu$ need not be any greater than that set by the intrinsic width of the features being observed (typically ∼1000 for unresolved galaxies). In practice $\mathcal{R}$ can be somewhat smaller without substantial degradation of performance, and a smaller $\mathcal{R}$ both reduces the number of detectors required and relaxes the required NEP. for a given bandwidth, thereby improving the efficiency of the instrument when it is detector-count-limited. For first-light X-Spec, we will field spectrometers with $\mathcal{R}$ between 400 (requirement) and 700 (goal).

Source densities – MOS vs IFU trade. We have considered two basic configurations: a multi-object steered-beam spectrometer (called MOS), similar to an optical multi-object spectrograph, and a simple imaging spectrometer (an integral field unit). In the MOS, a mechanism outside the cryostat tracks the source as it moves through the patrol region, with modulation provided by chopping to a reference position away from the source, either by moving the telescope in Azimuth, or with an on-board chopper. The imaging (referred to as IFU) system works like a camera, with modulation provided by scanning the telescope.

In the long-term limit of low-cost detectors and readouts, the on-chip technology enables close-packed coverage of the bulk of the 1 degree CCAT focal plane, so there is no benefit to the MOS. In the near-term, however, the cost of fabrication, screening, and reading out detectors remains dominant, and the realistic instrument scope is limited to a couple of hundred backends (few $\times 10^5$ KIDs). For the galaxy survey experiments, the density of sources selected for follow up will be between 0.001 and 0.1 per X-Spec beam. Identification of targets at higher densities is unlikely, since galaxies will be selected from long-wavelength continuum surveys: e.g. 850- μm surveys down to the confusion limit (so to a depth of 1/30 to 1/10 of a source per 850-μm beam). Moroever, the sources targeted for follow-up will be sub-samples of this parent population (e.g. the short-submm dropouts). For this class of follow-up spectroscopy, the IFU will be much less efficient than a steered-beam system. For the tomography experiment, there is no strong advantage to either the IFU or the MOS approach, so long as fields on order a degree in size are targeted, as is required to recover the 1- and 2-halo clustering signal.

Spectrometer Backend Requirements. Achieving the sensitivities shown in Figure 2 requires a wideband spectrometer backend which operates close to the photon background limit with an end-to-efficiency of ∼25% or better. Z-Spec is a proof of principle of the basic backend performance; Z-Spec's achieved on-sky sensitivities at the CSO in the 1-mm band are at the upper edge of the plotted range (and Z-Spec with $\mathcal{R}$ of 250 and single-polarization should be less sensitive than X-Spec at $\mathcal{R}$=400–700). The efficiency is crucial for good performance – even with perfect detectors, poor efficiency will degrade performance, so this is a major thrust of the on-chip spectrometer development. Detector sensitivities are also tabulated in Table 2, the required values are similar to what has been achieved in Z-Spec. As with Z-Spec, the designed detector loadings are as low as 3×10^{-14} W, requiring stray-light control. We have already demonstrated this control with our prototype chips.

Table 2. X-Spec System Parameters

Spectral coverage	Band 1: 190–320 GHz; Band 2: 330–520 GHz (dichroic and/or polarization diplexed)
Spectral resolving power	$\mathcal{R} = \nu/\delta\nu = 400$ – 700
# of detectors per spectrometer	500
# of spectrometer units	∼400 (4×84 = 336 for baseline steered system)
Total # of detectors	∼200,000 (170,000 for baseline steered system)
Loading and Photon NEP at Detector	$3–11\times10^{-14}$ W, $3–10\times10^{-18}$ W Hz$^{-1/2}$, at 190, 520 GHz
Steered-Beam Multi-Object Spectrometer: 84 beam concept	
Single-element patrol field	32 arcmin^2 = 0.01 deg^2
Survey speed vs. ALMA	6 times faster than full ALMA for galaxy redshift surveys at goal sensitivity
Telescope coupling	Horn-coupled to CCAT focus via steered relay
Focal plane footprint	2.8 m
Direct Imaging Spectrometer: 50 or 200 beams	
Diplexing	Dual-band via full-focal-plane grid
Telescope coupling	Reimaged to f/2.5
Pixel spacing	2.5λ at 240 GHz, square
Field size	e.g. 9 arcmin for 200 beams

3. ON-CHIP SPECTROMETER

X-Spec will employ new superconducting filterbank spectrometers with integrated KID arrays that are being developed by our group. The approach and our progress are described in detail in a paper by Hailey-Dunsheath et al. in these proceedings, as well in our previous publications.[23–25] We have demonstrated the essential filterbank functionality and are working to increase the net sensitivity of the devices. The current sensitivity at the front of the instrument for our Band-1 prototype is a factor of ∼10 from the performance of a background-limited R=100 spectrometer, and an additional factor of 2–3 from an X-Spec R=400–700 system. As Hailey-Dunsheath et al. note, the first factor of 10 is accessible with relatively straightforward adjustments to the existing design, specifically: 1) lower T_c for the TiN to increase response, 2) a smaller inductor, also to increase response (up to 4× is possible with 0.5-micron lines), and 3) improvements to the optical efficiency including an AR-coated lens and matching the filterbank-to-resonator and resonator-to-KID couplings.

While the KID sensitivity can be straightforwardly increased, a more fundamental adjustment required for the X-Spec chip the dielectric material. Internal losses in the dielectric reduce the power delivered to the detector by a factor $[1 - Q_{\rm tot}/Q_{\rm loss}]^2$, where $Q_{\rm tot}$ is the total Q of the channel. The silicon nitride we are currently using has $Q_{\rm loss} \sim 1440$, so half the power is lost to in the dielectric for $Q_{\rm tot} = 0.29\,Q_{\rm loss} \sim 420$. Thus, while suitable for a early-generation R∼100 experiment, pushing beyond R=400 as envisioned for X-Spec will require a different dielectric. Both crystalline silicon (such as Chuss et al. 2014[26]) and deposited amorphous silicon are under study; both should offer lower losses than the silicon nitride.

4. OPTICAL SYSTEM DESIGN

4.1 Multi-Object Spectrometer (MOS) Approach

We require an optical system capable of mapping a spectrometer feed horn onto a selectable location on the sky. At optical/NIR wavelengths this is typically achieved with a flexible optical fibre coupling a location in the telescope focal plane to a position in the spectrometer entrance slit, but at sub/millimeter wavelengths low-loss flexible waveguide technology does not yet exist. Instead, we will use an articulated quasioptical reimaging system, operating on the free space beam. The initial concept of the articulated feed was outlined by Goldsmith & Seiffert (2009).[27] The system has 4 mirrors with 2 rotational degrees of freedom, combined to form a double periscope placed in between the feed horn and the telescope (Figure 4). The upper and lower arms are rotated independently to translate the beam from the initial propagation direction to anywhere within a patrol region defined by the lengths of the two arms. A large number of these systems may be arrayed to divide the full telescope FOV into a number of separate patrol regions, each of which is accessed by a different feed. For more details see the Chapman et al. paper in these proceedings.

MOS Optical Prescription. The double periscope design requires 4 mirrors to steer the beam around the patrol region. The placement of these mirrors, the figure of each mirror, and the possibility of additional powered

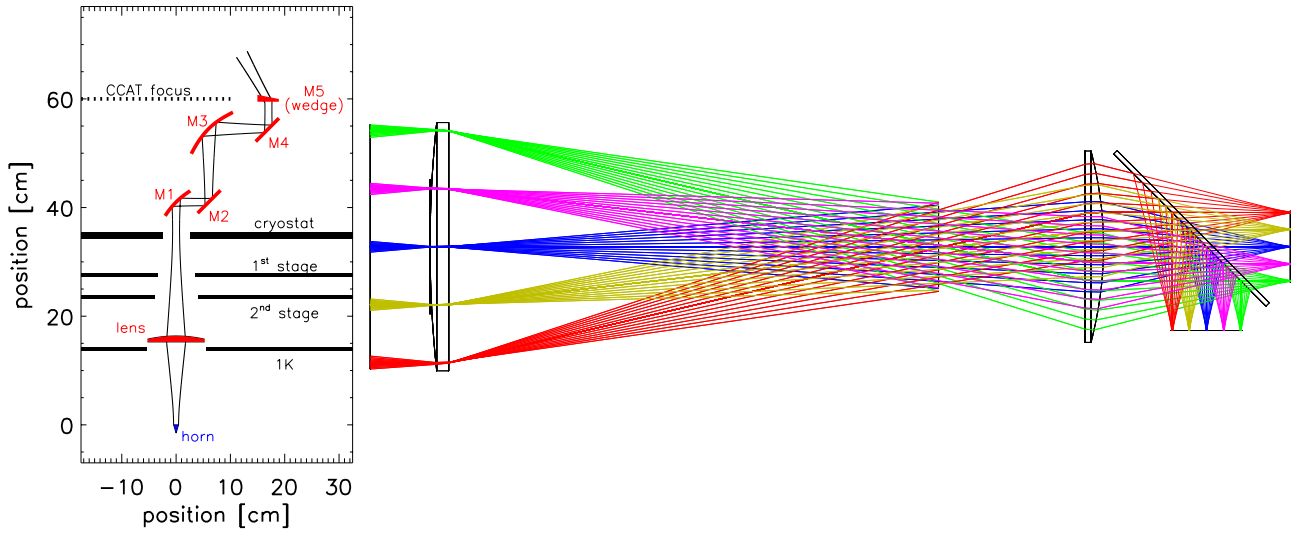

Figure 4. Optics design concepts for X-Spec. LEFT: Gaussian optics model for the MOS, including the two rotary stages. Radiation shields and the CCAT focal surface are flattened for clarity, only 1 of 4 horns are shown. RIGHT: IFU concept, adapted from the proposed LWCAM optical design. Radiation from the telescope is incident on the left, and a field lens and camera lens reimage to a 9′ diameter flat, telecentric focal plane, populated by a 200 beam module of band 1 chips. A dichroic inserted after the camera lens sends half the radiation to a second focal plane, populated by 200 band 2 chips. The objective lens is 46 cm and the focal plane size is 12 cm.

elements in the optical path are all free parameters that we have adjusted to insure a compact design with high efficiency, a small cryostat entrance window, and a small optic at the top of the positioner. Our approach is shown in Figure 4. A single cold lens is used to transform the beam waist formed at the horn to a reimaged waist at the position of the cryostat entrance window. Two of the four mirrors in the double periscope are powered, and form a Gaussian Beam Telescope (GBT) that reimages the waist at the cryostat entrance window to a waist at the output of the double periscope. The M5 wedge is placed at this waist, which is positioned at the telescope focal plane. We use a quasi-optical analysis to calculate the size of each element necessary to avoid vignetting the beam (we adopt a conservative requirement that each optic have a diameter of 6 times the beam radius at the longest wavelength). The spacing between M2 and M3 in the double periscope is set by the size of the MOS unit mechanical structure, while the M1 - M2 spacing is set to be as close as possible without vignetting the beam, and the M3 - M4 spacing is set by focal plane coverage considerations (see below).

Frequency Coverage – Polarization and Dichroic Splitting. Due to the large size of the individual patrol region (a 6′ diameter contains ≈800 diffraction-limited beams at 1.6mm), a large region of the focal plane is available to each individual MOS unit. To fully utilize this available space we choose to couple 4 spectrometer chips to each beam: for both polarizations we will have chips covering our band 1 ($190-310$ GHz) and band 2 ($330-540$ GHz). The incoming beam will first be split by a lithographically-defined polarizing grid, and for each polarization the beam will subsequently be split into the 2 bands with a metal-mesh dichroic. The cutoff of the dichroic is placed on the 325 GHz H_2O line to minimize the in-band efficiency losses near the transition. Bands will be defined with low-pass filters combined with waveguide cutoffs.

Anti-Reflection Coating. Our optical design aims to detect a large bandwidth through an optical train containing multiple transmissive optics, and as such we require the transmissive optics to have broad-band AR coating (ARC). For the steerable feed configuration we will have a cold lens, a flat cryostat entrance window, and a beam-steering wedge. For the IFU configuration we will have 3 lenses. In both cases, we require transmission better than 90% in Bands 1 and 2 (190–520 GHz). Silicon is sufficiently low loss, and simulations suggest that 2 layers, either coatings or machined structures,[28] are sufficient to provide <1% reflection per surface.

Beam Switching for MOS. With no chopping secondary, we need an alternate means of modulating the sky signal faster than the 1/f knee of the atmospheric noise. One method is simply to nod the entire telescope as rapidly as possible. The CCAT telescope servo model suggests a 3 beam nod at 1mm can be achieved at 0.25 Hz

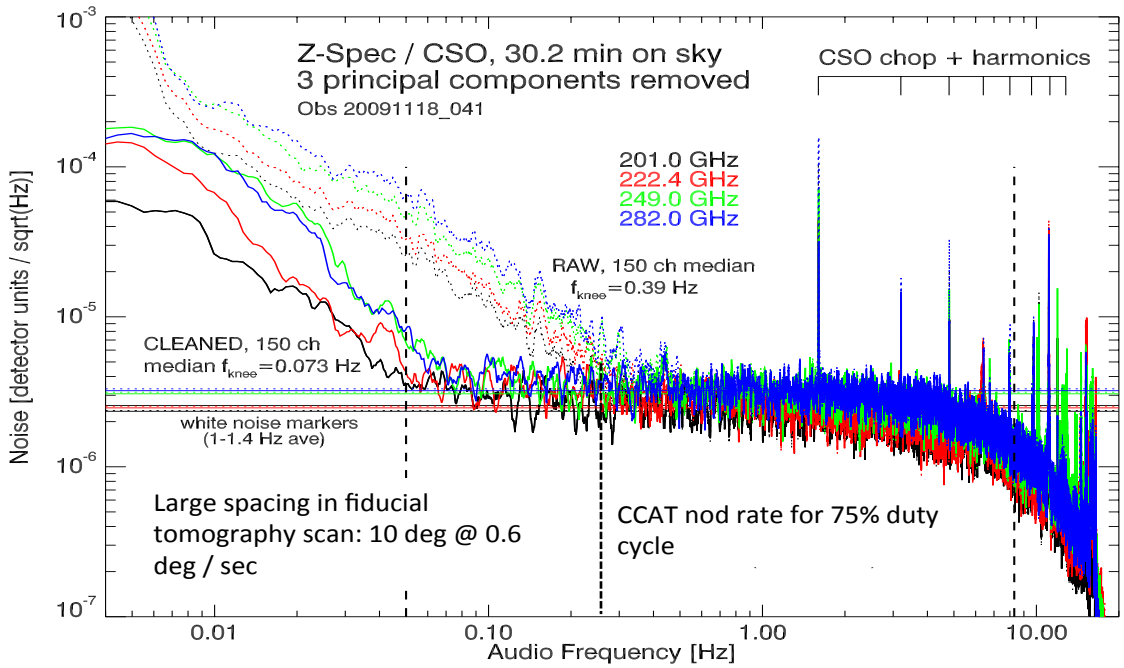

Figure 5. Sky fluctuation noise as measured with Z-Spec at the CSO. Dotted lines show the raw power spectral density (PSD) of four $\mathcal{R}$=300 channels. Solid lines show the data after removal of 3 principal components obtained by using the full 160-channel spectrometer to remove correlated noise. These data indicate that it may not be necessary to modulate faster than 0.1 Hz, in which case the telescope can simply nod in azimuth.

with 75% efficiency. Existing Z-Spec data from the CSO suggest the knee in the raw sky noise is ≈0.4 Hz, but with common mode subtraction, this may be reduced to ≈0.04Hz, as shown in Figure 5. Thus a simple telescope nodding should be sufficient, but we are studying as a fallback an integrated chopping mirror in the positioner.

4.2 Integral-Field Unit (IFU) Design

An alternative to the steerable system is to pack a number of spectrometers into a filled focal plane to form an integral field unit (IFU) spectrometer. In this case it is preferable to combine the spectrometer chips into a large module, and hence to reimage a segment of the curved CCAT focal plane into a flat and telecentric focus. The CCAT LWCam team has discovered a reimaging solution that uses 2 silicon lens to flatten a 9′ diameter section of the CCAT FOV, with good imaging quality and telecentricity (Figure 4). The X-Spec IFU will combining enough chips to fully populate this FOV—our feed horn allows spacing beams by $\approx 2.6F\lambda$, and with this spacing at our longest wavelength $\lambda = 1.6$mm the 9′ FOV will allow ≈200 horns. We will take full advantage of this available FOV by splitting the radiation with a polarizing grid and inserting a second focal plane, with horns and chips designed for our band 2. This enables a 200-beam IFU with full coverage from $190 - 520$ GHz.

5. CRYOSTAT AND MECHANICAL CONFIGURATION

4-Chip Spectrometer Module. Each of the positioner mechanisms couples to a backend spectrometer module within the cryostat. Each module houses 4 chips, one each for Bands 1 and 2 in the two polarizations. While on-chip diplexers could be considered, each polarization requires a separate filterbank regardless of the coupling scheme, and the single-polarization-per-chip approach minimizes the requirements on the already-challenging superconducting circuit. The concept for the backend module is shown in Figure 6; each consists of two dual-chip blocks on either side of a polarizing grid. The spectrometer chip housing is made of E-plane split block so that the waveguide sections can be directly machined in. The feedhorns are then drilled into the assembled waveguide block using a custom-ground bit as pioneered by Leech et al. (2011).[29]

Cryostat and Thermal System Design. The cryostat concept for the MOS is shown in Figure 7. It is designed to occupy the full 1-degree (∼3-meter) field on one of the CCAT Nasmyth platforms. The frontispiece is formed from a spun head welded to a cylindrical body and flange, and is machined to provide accurate mounting

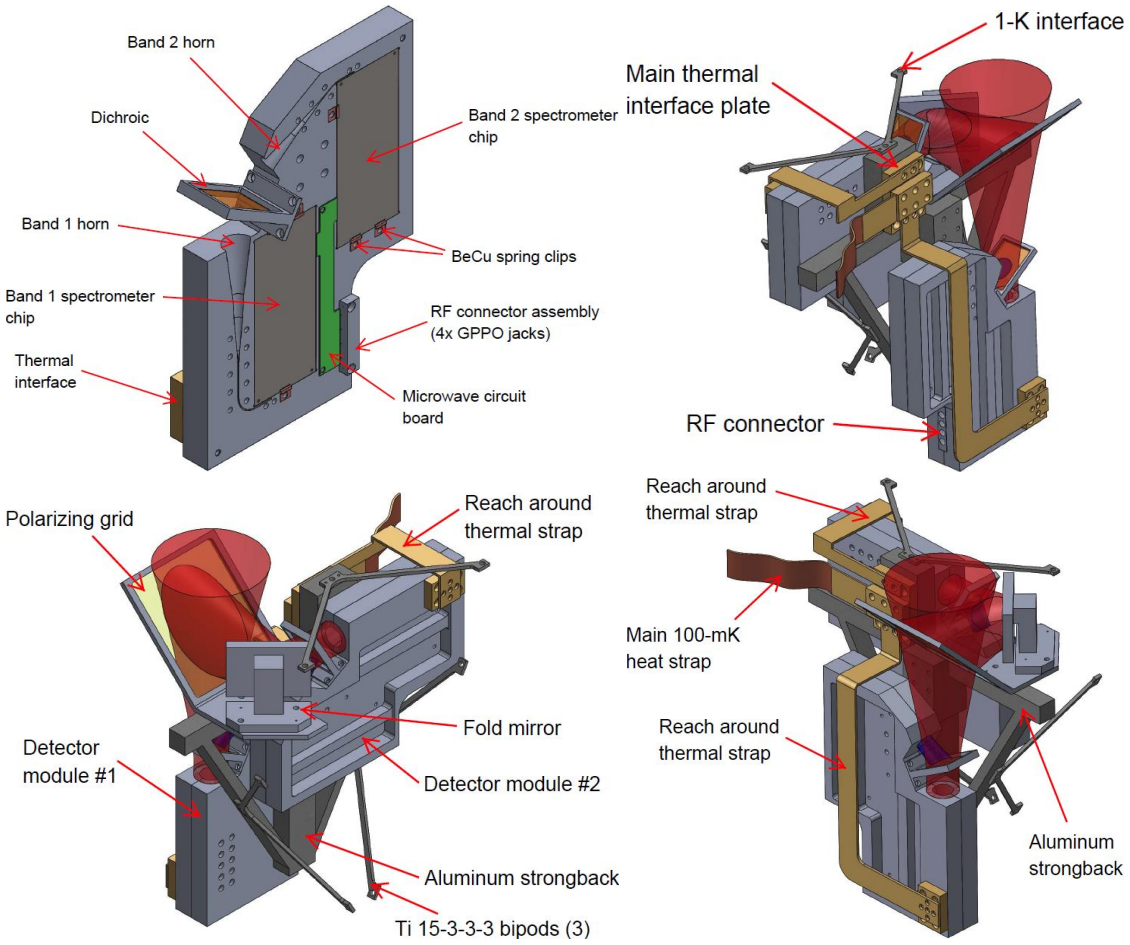

Figure 6. Dual-band, dual-pol 4-chip spectrometer module. Upper left shows the 2-chip housing made of E-plane split-block waveguide, with integrated smooth-wall direct-drilled feed horns and a dichroic. The other images show the full 4-chip module including 2 dual-chip housings and the polarizing grid. Red shows Gaussian beams sized at $4w$ for $\lambda = 1.6$ mm, blue for $\lambda = 0.91$ mm, the long-wavelength ends of Band 1 and Band 2, respectively.

surfaces for the positioner mechanisms and the silicon vacuum windows. There are three curved radiation shields interior to the vacuum with mount positions for filters at each penetration. The system uses two Cryomech PT415 coolers and two PT815 coolers, providing a total lift of approximately 280 W at 60 K, 14 W at 8 K and 3 W at 4 K. This configuration is easily sufficient to support the 84-element MOS systems, and would also be suitable for the large IFU systems with several thousand beams. The sub-K cooling is provided by a commercial closed-cycle dilution cooler which can easily handle the estimated 140μW of conducted load to 100 mK. With an estimated mass of 4 tons, the full system is large, but within the CCAT instrument allocation.

ACKNOWLEDGMENTS

We thank Yang Gong and Asantha Cooray for the X-Spec [CII] intensity mapping calculations.

REFERENCES

1. C. M. Casey, C.-C. Chen, L. Cowie, A. Barger, P. Capak, O. Ilbert, M. Koss, N. Lee, E. Le Floc'h, D. B. Sanders, and J. P. Williams, "Characterisation of SCUBA-2 450um and 850um-selected Galaxies in the COSMOS Field," *ArXiv e-prints* , Feb. 2013.
2. R. J. Bouwens, G. D. Illingworth, P. A. Oesch, I. Labbé, M. Trenti, P. van Dokkum, M. Franx, M. Stiavelli, C. M. Carollo, D. Magee, and V. Gonzalez, "Ultraviolet Luminosity Functions from 132 z ˜ 7 and

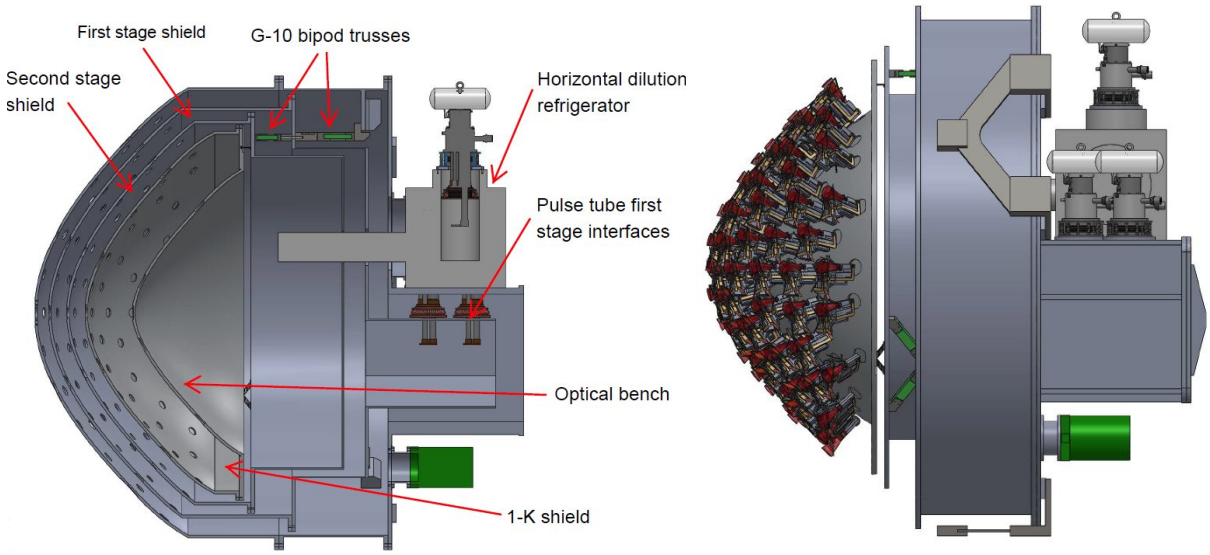

Figure 7. X-Spec cryostat, 84-element steered system configuration. The maximum diameter of the cylindrical jacket is 260 cm, and the full length is 278 cm. Positioners are not shown, and the positions of the vacuum jacket feeds and the 4-chip modules are not updated to reflect the latest positioning described in Section 4.

z ˜ 8 Lyman-break Galaxies in the Ultra-deep HUDF09 and Wide-area Early Release Science WFC3/IR Observations," *ApJ* **737**, p. 90, Aug. 2011.

3. D. J. Fixsen, E. Dwek, J. C. Mather, C. L. Bennett, and R. A. Shafer, "The spectrum of the extragalactic far-infrared background from the COBE FIRAS observations," **508**, pp. 123–128, Nov. 1998.
4. C. M. Bradford, J. E. Aguirre, R. Aikin, J. J. Bock, L. Earle, J. Glenn, H. Inami, P. R. Maloney, H. Matsuhara, B. J. Naylor, H. T. Nguyen, and J. Zmuidzinas, "The Warm Molecular Gas around the Cloverleaf Quasar," *ApJ* **705**, pp. 112–122, Nov. 2009.
5. L. Spinoglio, K. M. Dasyra, A. Franceschini, C. Gruppioni, E. Valiante, and K. Isaak, "Far-IR/Submillimeter Spectroscopic Cosmological Surveys: Predictions of Infrared Line Luminosity Functions for z < 4 Galaxies," *ApJ* **745**, p. 171, Feb. 2012.
6. E. Visbal, H. Trac, and A. Loeb, "Demonstrating the feasibility of line intensity mapping using mock data of galaxy clustering from simulations," *J. Cos. Astroparticle Phys* **8**, pp. 10–+, Aug. 2011.
7. S. Hailey-Dunsheath, T. Nikola, G. J. Stacey, T. E. Oberst, S. C. Parshley, D. J. Benford, J. G. Staguhn, and C. E. Tucker, "Detection of the 158 μm [C II] Transition at z = 1.3: Evidence for a Galaxy-wide Starburst," *ApJL* **714**, pp. L162–L166, May 2010.
8. G. J. Stacey, S. Hailey-Dunsheath, C. Ferkinhoff, T. Nikola, S. C. Parshley, D. J. Benford, J. G. Staguhn, and N. Fiolet, "A 158 μm [C II] Line Survey of Galaxies at z ˜ 1-2: An Indicator of Star Formation in the Early Universe," *ApJ* **724**, pp. 957–974, Dec. 2010.
9. J. Graciá-Carpio, E. Sturm, S. Hailey-Dunsheath, J. Fischer, A. Contursi, A. Poglitsch, R. Genzel, E. González-Alfonso, A. Sternberg, A. Verma, N. Christopher, R. Davies, H. Feuchtgruber, J. A. de Jong, D. Lutz, and L. J. Tacconi, "Far-infrared Line Deficits in Galaxies with Extreme L_{FIR}/M_{H_{2}} Ratios," *ApJL* **728**, p. L7, Feb. 2011.
10. T. Díaz-Santos, L. Armus, V. Charmandaris, S. Stierwalt, E. J. Murphy, S. Haan, H. Inami, S. Malhotra, R. Meijerink, G. Stacey, A. O. Petric, A. S. Evans, S. Veilleux, P. P. van der Werf, S. Lord, N. Lu, J. H. Howell, P. Appleton, J. M. Mazzarella, J. A. Surace, C. K. Xu, B. Schulz, D. B. Sanders, C. Bridge, B. H. P. Chan, D. T. Frayer, K. Iwasawa, J. Melbourne, and E. Sturm, "Explaining the [C II]157.7 μm Deficit in Luminous Infrared Galaxies–First Results from a Herschel/PACS Study of the GOALS Sample," *ApJ* **774**, p. 68, Sept. 2013.
11. R. J. Bouwens, G. D. Illingworth, M. Franx, and H. Ford, "z ˜ 7-10 Galaxies in the HUDF and GOODS Fields: UV Luminosity Functions," *ApJ* **686**, pp. 230–250, Oct. 2008.

12. R. Salvaterra, A. Ferrara, and P. Dayal, "Simulating high-redshift galaxies," *MNRAS* **414**, pp. 847–859, June 2011.
13. T.-C. Chang, U.-L. Pen, K. Bandura, and J. B. Peterson, "Hydrogen 21-cm Intensity Mapping at redshift 0.8," *ArXiv e-prints* , July 2010.
14. C. L. Carilli, "Intensity Mapping of Molecular Gas During Cosmic Reionization," *ApJL* **730**, p. L30, Apr. 2011.
15. E. Visbal and A. Loeb, "Measuring the 3D clustering of undetected galaxies through cross correlation of their cumulative flux fluctuations from multiple spectral lines," *J. Cos. Astroparticle Phys* **11**, p. 16, Nov. 2010.
16. Y. Gong, A. Cooray, M. B. Silva, M. G. Santos, and P. Lubin, "Probing Reionization with Intensity Mapping of Molecular and Fine-structure Lines," *ApJL* **728**, p. L46, Feb. 2011.
17. Y. Gong, A. Cooray, M. Silva, M. G. Santos, J. Bock, C. M. Bradford, and M. Zemcov, "Intensity Mapping of the [C II] Fine Structure Line during the Epoch of Reionization," *ApJ* **745**, p. 49, Jan. 2012.
18. A. Lidz, S. R. Furlanetto, S. P. Oh, J. Aguirre, T.-C. Chang, O. Doré, and J. R. Pritchard, "Intensity Mapping with Carbon Monoxide Emission Lines and the Redshifted 21 cm Line," *ApJ* **741**, p. 70, Nov. 2011.
19. Y. Gong, A. Cooray, M. Silva, M. G. Santos, J. Bock, C. M. Bradford, and M. Zemcov, "Intensity Mapping of the [C II] Fine Structure Line during the Epoch of Reionization," *ApJ* **745**, p. 49, Jan. 2012.
20. P. Madau, A. Meiksin, and M. J. Rees, "21 Centimeter Tomography of the Intergalactic Medium at High Redshift," *ApJ* **475**, p. 429, Feb. 1997.
21. A. Loeb and M. Zaldarriaga, "Measuring the Small-Scale Power Spectrum of Cosmic Density Fluctuations through 21cm Tomography Prior to the Epoch of Structure Formation," *Physical Review Letters* **92**, p. 211301, May 2004.
22. N. Y. Gnedin and P. A. Shaver, "Redshifted 21 Centimeter Emission from the Pre-Reionization Era. I. Mean Signal and Linear Fluctuations," *ApJ* **608**, pp. 611–621, June 2004.
23. E. Shirokoff, P. S. Barry, C. M. Bradford, G. Chattopadhyay, P. Day, S. Doyle, S. Hailey-Dunsheath, M. I. Hollister, A. Kovács, C. McKenney, H. G. Leduc, N. Llombart, D. P. Marrone, P. Mauskopf, R. O'Brient, S. Padin, T. Reck, L. J. Swenson, and J. Zmuidzinas, "MKID development for SuperSpec: an on-chip, mm-wave, filter-bank spectrometer," in *Society of Photo-Optical Instrumentation Engineers (SPIE) Conference Series*, *Society of Photo-Optical Instrumentation Engineers (SPIE) Conference Series* **8452**, Sept. 2012.
24. E. Shirokoff, P. Barry, C. Bradford, G. Chattopadhyay, P. Day, S. Doyle, S. Hailey-Dunsheath, M. Hollister, A. Kovács, H. Leduc, C. McKenney, P. Mauskopf, H. Nguyen, R. O'Brient, S. Padin, T. Reck, L. Swenson, C. Tucker, and J. Zmuidzinas, "Design and performance of superspec: An on-chip, kid-based, mm-wavelength spectrometer," *Journal of Low Temperature Physics* , pp. 1–6, 2014.
25. S. Hailey-Dunsheath, P. Barry, C. Bradford, G. Chattopadhyay, P. Day, S. Doyle, M. Hollister, A. Kovacs, H. LeDuc, N. Llombart, P. Mauskopf, C. McKenney, R. Monroe, H. Nguyen, R. O'Brient, S. Padin, T. Reck, E. Shirokoff, L. Swenson, C. Tucker, and J. Zmuidzinas, "Optical measurements of superspec: A millimeter-wave on-chip spectrometer," *Journal of Low Temperature Physics* , pp. 1–7, 2014.
26. D. T. Chuss, A. Ali, J. W. Appel, C. L. Bennett, F. Colazo, E. Crowe, K. Denis, J. Eimer, T. Essinger-Hileman, T. Marriage, S. H. Moseley, K. Rostem, T. Stevenson, D. Towner, K. U-Yen, E. Wollack, and L. Zeng, "Feedhorn-coupled Bolometer Detectors at 40 GHz Implemented on the Cosmology Large Angular Scale Surveyor (CLASS)," in *American Astronomical Society Meeting Abstracts #223*, *American Astronomical Society Meeting Abstracts* **223**, p. 439.03, Jan. 2014.
27. P. F. Goldsmith and M. Seiffert, "A Flexible Quasioptical Input System for a Submillimeter Multiobject Spectrometer," *PASP* **121**, pp. 735–742, July 2009.
28. R. Datta, C. D. Munson, M. D. Niemack, J. J. McMahon, J. Britton, E. J. Wollack, J. Beall, M. J. Devlin, J. Fowler, P. Gallardo, J. Hubmayr, K. Irwin, L. Newburgh, J. P. Nibarger, L. Page, M. A. Quijada, B. L. Schmitt, S. T. Staggs, R. Thornton, and L. Zhang, "Large-aperture wide-bandwidth antireflection-coated silicon lenses for millimeter wavelengths," *Applied Optics* **52**, p. 8747, Dec. 2013.
29. J. Leech, B. K. Tan, G. Yassin, P. Kittara, S. Wangsuya, J. Treuttel, M. Henry, M. L. Oldfield, and P. G. Huggard, "Multiple flare-angle horn feeds for sub-mm astronomy and cosmic microwave background experiments," *A&A* **532**, p. A61, Aug. 2011.